Microscopic calculation of in-medium proton-proton cross sections

G. Q. Li* and R. Machleidt
Department of Physics, University of Idaho, Moscow, Idaho 83843
(Received 12 August 1993)

We derive in-medium *proton-proton* cross sections in a microscopic model based upon the Bonn nucleon-nucleon potential and the Dirac-Brueckner approach for nuclear matter. We demonstrate the difference between proton-proton and neutron-proton cross sections and point out the need to distinguish carefully between the two cases. We also find substantial differences between our in-medium cross sections and phenomenological parametrizations that are commonly used in heavy-ion reactions.

PACS number(s): 21.65.+f, 21.30.+y

The density and/or temperature dependence of hadronic systems is an interesting topic in nuclear physics. Experimentally, nucleus-nucleus collisions at intermediate energies provide a unique opportunity to form a piece of hot nuclear matter in the laboratory with a density up to 2–3ρ_0 (with ρ_0, in the range of 0.15–0.19 fm^{-3}, the saturation density of normal nuclear matter; in this paper we use ρ_0=0.18 fm^{-3}) [1,2]. It is thus possible to study the properties of hadrons in hot and dense medium. Since this piece of dense nuclear matter exists only for a very short time (typically 10^{-23}–10^{-22} s), it is necessary to use transport models to simulate the entire collision process and to deduce the properties of the intermediate stage from the known initial conditions and the final-state observables. At intermediate energies, both the mean field and the two-body collisions play an equally important role in the dynamical evolution of the colliding system; they have to be taken into account in the transport models on an equal footing, together with a proper treatment of the Pauli blocking for the in-medium two-body collisions. The Boltzmann-Uehling-Uhlenbeck (BUU) equation [3,4] and quantum molecular dynamics (QMD) [5,6], as well as their relativistic extensions (RBUU and RQMD), are promising transport models for the description of intermediate-energy heavy-ion reactions.

Starting from the bare nucleon-nucleon (NN) interaction, in-medium NN cross sections have been calculated using relativistic [7,8] as well as nonrelativistic [9,10] Brueckner theory. In Ref. [8], we derived microscopically the in-medium *neutron-proton* (np) cross sections. Our derivation was based on the Bonn meson-exchange model for the NN interaction [11,12] and the Dirac-Brueckner approach [12–14] for nuclear matter. We found that our microscopic in-medium np cross sections deviate substantially from the phenomenological parametrization by Cugnon *et al.* [15] which is often used in transport model calculations [3–6].

In this Brief Report, we present now our microscopic results for in-medium *proton-proton* (pp) cross sections. The original Cugnon parametrization of NN cross sections [15], which is discussed in detail in Ref. [3], is, in fact, a fit of the free-space pp data; i.e., no difference is made between np and pp scattering. Recently, Cugnon and Lemaire [16] have developed a new parametrization that distinguishes between pp and np; but again only the free-space scattering data are described. These isospin-dependent Cugnon parametrizations for NN cross sections have been used in some recent transport model calculations (see, e.g., Ref. [6]). Our results will show that there are sizable medium effects on the pp cross sections and that there are important differences between pp and np, also in the medium.

Proton-proton scattering occurs only in states of total isospin $T = 1$, while np exists for T =0 and 1. This fact is responsible for the characteristic differences in the shapes of pp and np differential cross sections. This is the most crucial difference between pp and np and should by no means be ignored. Furthermore, there is the Coulomb force which is involved in pp but not in np. Finally, in the $^1S_0$ state, the strength of the strong interaction shows a small difference between pp and np which is known as charge-independence breaking (CIB). However, this is a very small effect and totally negligible in our present considerations: The in-medium effects are by an order of magnitude larger than CIB.

In general, in transport models such as BUU and QMD, the electromagnetic effects between nucleons, mainly the Coulomb interaction, are treated separately. So, for the treatment of pp scattering in the transport models, what is needed are the in-medium pp cross sections due to the strong force only. Therefore, we calculate in this paper the pp cross sections without the Coulomb force. Then, the main difference between pp and np cross sections is due to the fact that in the former case only the $T = 1$ NN channels are included while in the latter case all $T = 0$ and $T = 1$ states are taken into account. We note that our pp cross sections can also be used as neutron-neutron (nn) cross sections, since we neglect electromagnetic effects anyhow and the small charge-symmentry breaking (CSB), i.e., the small difference between the pp and nn strong force, is totally negligible here (cf. our remark, above, concerning CIB).

In this paper, we apply exactly the the same methods as in our earlier (and more detailed) paper [8] about np

*Present address: Cyclotron Institute, Texas A&M University, College Station, TX 77843.

cross sections to which we refer the interested reader for details. It is therefore sufficient to just sketch our method briefly here. We start from the relativistic one-boson-exchange (OBE) Bonn potential [12] which describes the two-nucleon system below 300 MeV accurately. This potential is used in (relativistic) Dirac-Brueckner calculation for nuclear matter, in which also the effective nucleon scalar and vector fields (the mean field) are determined. With this nucleon mean field and the Lorentz-boosted Pauli projector, we solve the in-medium Thompson equation (relativistic Bethe-Goldstone equation) to determine the $\tilde{G}$ matrix, from which the in-medium NN cross sections are calculted by identifying the $\tilde{G}$ matrix with the in-medium K matrix. As in Ref. [8], we present our results in terms of the kinetic energy of the incident nucleon in the "laboratory system" (E_{lab}) in which the second nucleon is at rest. All results shown in this paper are obtained by using the Bonn A potential [12] for the bare nuclear force; in Ref. [8] we have shown that the dependence of our results on the particular model for the nuclear force is very small (as long as the model is quantitative and relativistic).

In Fig. 1, we show the differential cross section at E_{lab}=50 (a) and 200 MeV (b) for three different densities [$\rho = 0$ (solid curves), $\rho = \rho_0$ (dashed curves), and $\rho = 2\rho_0$ (dotted curves)]. At 50 MeV, the in-medium differential cross section decreases with increasing density. At 250 MeV, it decreases when going from $\rho = 0$ to $\rho = \rho_0$ and then increases. We observed a similar behavior in np [8]. The reason for this is that with increasing energy, the higher partial waves become more important which are less influenced by medium effects. As in the case of the np differential cross sections [8], we have prepared a data file, containing the pp differential cross sections as a function of angle, for a number of energies and densities. From this data file, the pp differential cross sections for any density between 0 and $3\rho_0$ and any energy between 0 and 300 MeV can be obtained with sufficient accuracy by interpolation. This data file is available from the authors upon request.

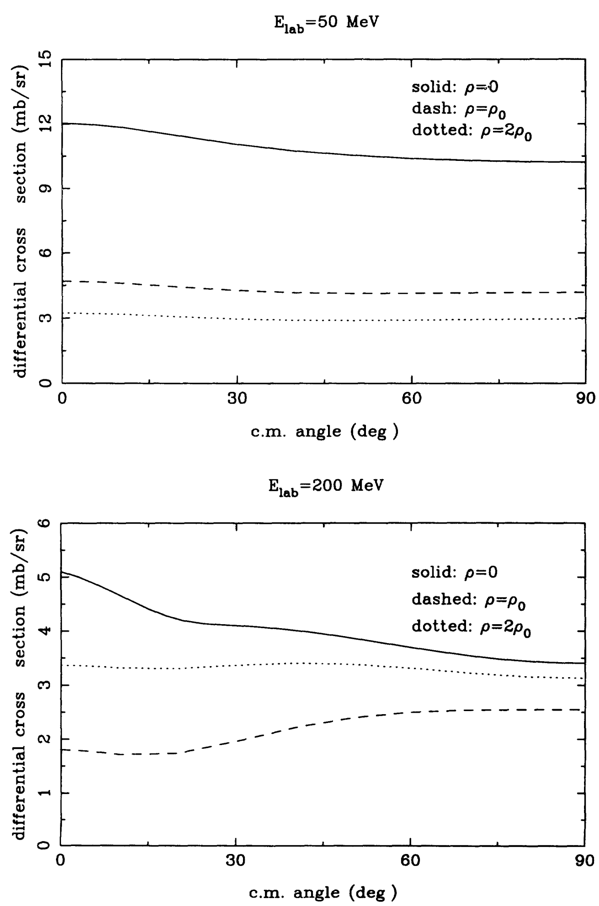

FIG. 1. In-medium pp differential cross sections at (a) 50 MeV and (b) 200 MeV laboratory energy. Three densities are considered: $\rho = 0$ (solid line), $\rho = \rho_0$ (dashed line), and $\rho = 2\rho_0$ (dotted line) ($\rho_0 \equiv 0.18$ fm^{-3}).

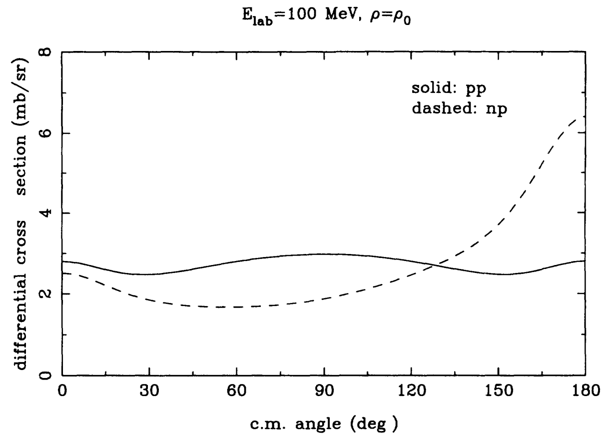

FIG. 2. In-medium pp and np differential cross sections at 100 MeV laboratory energy for the density $\rho = \rho_0 = 0.18$ fm^{-3}.

In Fig. 2, we compare the pp differential cross section with the np one at E_{lab}=100 MeV and ρ=ρ_0. Clearly there are differences between pp and np. The pp differential cross section is almost isotropic and has the symmetry of $d\sigma/d\Omega(\theta) = d\sigma/d\Omega(\pi - \theta)$, while the np differential cross section is highly anisotropic and has a profound

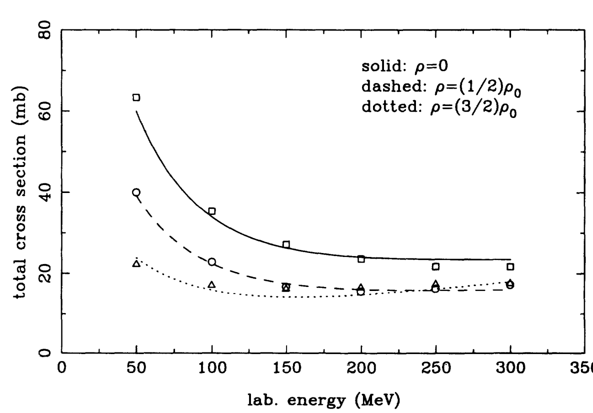

FIG. 3. In-medium pp total cross sections as function of incident energy for three densities. The symbols represent the results of our exact calculations while the curves are fits of our results in terms of the ansatz Eq. (1).

TABLE I. Microscopic in-medium *pp* total cross sections in units of mb as derived in the present work ($\rho_0 \equiv 0.18$ fm^{-3}).

ρ	$E_{\rm lab}$ (MeV) 50	100	150	200	250	300
0	63.38	35.36	27.18	23.62	21.76	21.72
$(1/2)\rho_0$	40.03	22.84	16.75	15.59	16.29	17.28
ρ_0	26.37	17.36	14.73	14.80	15.33	16.00
$(3/2)\rho_0$	22.24	17.06	16.19	16.52	17.37	17.61
$2\rho_0$	18.50	18.60	21.06	20.61	20.35	20.10

peak at backward angles. This difference is mainly due to the fact that the $T = 0$ states do not contribute to *pp*. In summary, Fig. 2 demonstrates, from a microscopic point of view, that one should distinguish carefully between *pp* and *np* cross sections.

In Fig. 3, we show the *pp total* cross sections as a function of the incident energy, at ρ=0 (solid curves), $(1/2)\rho_0$ (dashed curves), and $(3/2)\rho_0$ (dotted curves). The symbols represent the exact results of our microscopic calculation, while the curves are fits in terms of a simple and practical parametrization of our results:

$$\sigma_{pp}(E_{\rm lab},\rho) = [23.5 + 0.0256(18.2 - E_{\rm lab}^{0.5})^{4.0}] \times \frac{1.0 + 0.1667 E_{\rm lab}^{1.05}\rho^3}{1.0 + 9.704\rho^{1.2}}, \tag{1}$$

where $E_{\rm lab}$ and ρ are in units of MeV and fm^{-3}, respectively. Generaly speaking, the in-medium *pp* total cross sections decrease with increasing density and energy. For completeness, we list in Table I the in-medium *pp* total cross sections as function of energy and density for some selected values.

Finally, in Fig. 4, we compare the *pp* total cross section with the *np* one at $\rho = 0$ (a) and $(3/2)\rho_0$ (b). Also shown is the description by the orignal Cugnon parametrization given in Ref. [15]. Notice that at ρ=0 [Fig. 4(a)], our results for the *pp* total cross section is very close to the one by Cugnon *et al.* This makes sense since the original Cugnon parametrization is a fit of the Coulomb subtracted free-space *pp* scattering data. At this point, we note that, since the in-medium *pp* cross section is always smaller than the free one (see Fig. 3), the Cugnon parametrization overestimates the in-medium NN cross sections. Figure 4(a) clearly demonstrates the difference between *pp* and *np* total cross sections. The *np* cross sections are much larger than the *pp* ones, especially at low energies and densities. At finite densities, this difference is reduced, since the $^3S_1$ amplitude, which contributes only in *np*, is considerably quenched in the medium. However, the in-medium *np* and *pp* cross sections still show appreciable differences and should be carefully distinguished when they are used in the transport models.

In summary, we have presented in this Brief Report predictions for in-medium *pp* cross sections derived in a microscopic way. The important conclusions are the following.

(1) There is strong density dependence in the in-medium cross sections. Cross sections decrease in the medium. This indicates that a proper treatment of the density dependence of the in-medium NN cross sections is important, when in-medium NN scattering is treated in the transport models.

(2) Our microscopic predictions for free-space *pp* cross sections are close to the parametrization developed by Cugnon *et al.* [3,15]. However, at finite densities which are important in transport models, the Cugnon parametrization, which is density independent, overestimates the cross sections.

(3) There are substantial differences between *pp* and *np* cross sections (total as well as differential) both in free space and in the nuclear medium. This implies that one should carefully distinguish between *pp* and *np* scattering when applying NN cross sections in transport models.

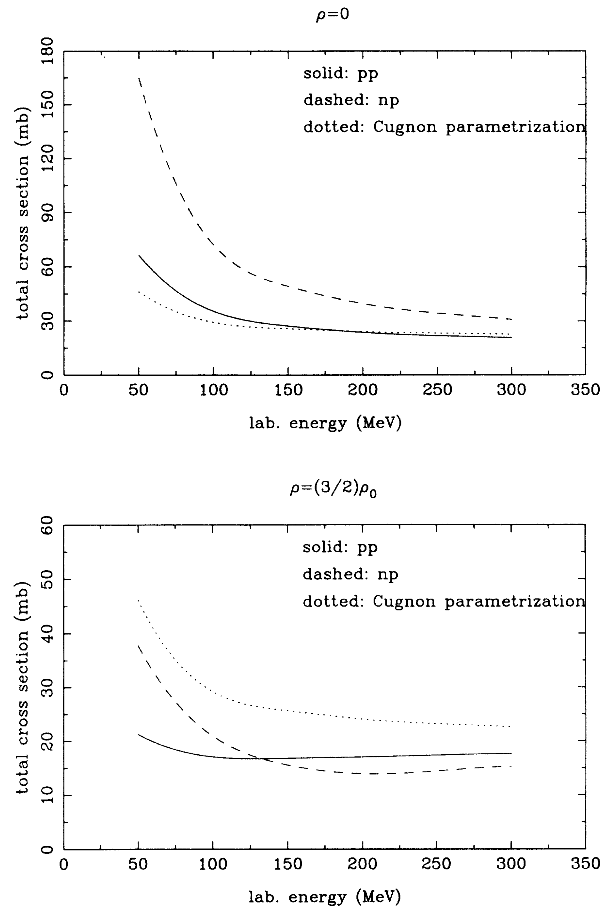

FIG. 4. The in-medium *pp* and *np* total cross sections at (a) ρ=0 and (b) $\rho = (3/2)\rho_0$ as obtained in our microscopic derivation (solid and dashed lines, respectively) are compared to the description of NN cross sections by the Cugnon parametrization.

One of the authors (G.Q.L.) gratefully acknowledges enlightening discussions with Professor C. M. Ko. This work was supported in part by the U.S. National Science Foundation under Grant No. PHY-9211607, and by the Idaho State Board of Education.

[1] R. Stock, Phys. Rep. **135**, 259 (1986).
[2] H. Stöcker and W. Greiner, Phys. Rep. **137**, 278 (1986).
[3] G. F. Bertsch and S. Das Gupta, Phys. Rep. **160**, 189 (1988).
[4] W. Cassing, W. Metag, U. Mosel, and K. Niita, Phys. Rep. **188**, 363 (1990).
[5] J. Aichelin and H. Stöcker, Phys. Lett. B **176**, 14 (1986).
[6] J. Aichelin, Phys. Rep. **202**, 235 (1991).
[7] B. ter Haar and R. Malfliet, Phys. Rev. C **36**, 1611 (1987).
[8] G. Q. Li and R. Machleidt, Phys. Rev. C **48**, 1702 (1993).
[9] A. Bohnet, N. Ohtsuka, J. Aichelin, R. Linden, and A. Faessler, Nucl. Phys. **A494**, 349 (1989).
[10] J. Jänicke, J. Aichelin, N. Ohtsuka, R. Linden, and A. Faessler, Nucl. Phys. **A536**, 201 (1992).
[11] R. Machleidt, K. Holinde, and Ch. Elster, Phys. Rep. **149**, 1 (1987).
[12] R. Machleidt, Adv. Nucl. Phys. **19**, 189 (1989).
[13] R. Brockmann and R. Machleidt, Phys. Rev. C **42**, 1965 (1990).
[14] G. Q. Li, R. Machleidt, and R. Brockmann, Phys. Rev. C **45**, 2782 (1992).
[15] J. Cugnon, T. Mitutani, and J. Vandermeulen, Nucl. Phys. **A352**, 505 (1981).
[16] J. Cugnon and M.-C. Lemaire, Nucl. Phys. **A489**, 781 (1988).